Egypt. J. Chem. **Vol. 68**, No. 3 pp. 569 - 583 (2025)

Egyptian Journal of Chemistry

http://ejchem.journals.ekb.eg/

Development of a Nanostructured Hydrazinyl Schiff Base Co(II) Complex-Functionalized Quartz Crystal Microbalance Sensor for Trace-Level Arsenic Detection in Aqueous Systems

Omnia M. Fahmy [1*], Rasha M. Elnashar [1], Walaa H. Mahmoud [1], Ahmed A. El-Sherif [1]

[1]*Chemistry Department, Faculty of Science, Cairo University, Giza, 12613 Egypt*

Abstract

In recent times, there has been a significant rise in global arsenic intake, stemming from both drinking water and food sources. Arsenic contamination in groundwater can originate from natural geological processes and anthropogenic activities such as industrial effluents, agricultural practices like insecticide use, municipal sewage, and household waste. One eco-friendly and dependable method for addressing this issue involves the synthesis of metal complex nanoparticles, which have broad applications in various fields, including sensing, catalysis, and environmental remediation. A noteworthy development is the creation of a novel nano-hydrazinyl Schiff base Co(II) complex sensor designed specifically for detecting arsenic with high sensitivity and selectivity. This nano-hydrazinyl Schiff base Co(II) complex underwent comprehensive characterization using a range of analytical tools, including Dynamic Light Scattering (DLS), Zeta potential analysis, Transmission Electron Microscopy (TEM), Scanning Electron Microscopy (SEM), Fourier-Transform Infrared Spectroscopy (FT-IR), contact angle measurements, as well as BET surface area and pore size determination. The nanoparticles exhibited excellent water dispersibility, high surface area, and favorable hydrophobic properties, making them suitable for sensing applications in aqueous environments. Furthermore, researchers explored the practical application of the Nano Hydrazinyl Schiff Base Co(II) Complex as a simple, cost-effective, and highly sensitive Quartz Crystal Microbalance (QCM) sensor for rapidly detecting arsenic. Using this Nano Hydrazinyl Schiff Base Co(II) Complex sensor, arsenic can be reliably detected even at deficient concentrations, as low as 1 ppm, with a remarkable response time of 7-8 minutes. Additionally, the cytotoxicity of the Hydrazinyl Schiff Base Co(II) Complex nanoparticles was thoroughly investigated to ensure their safety. This innovative method has demonstrated its effectiveness and feasibility for precisely determining arsenic ions in groundwater and industrial effluent wastewater samples.

Keywords: Arsenic ; Nanoparticles; QCM sensor; Schiff base; Cobalt complex; Nanosensor

1. Introduction

Arsenic, a ubiquitous and highly toxic trace element, poses a severe environmental and public health concern even at minuscule concentrations [1]. Its toxicity stems from its ability to bind to and inhibit enzymes crucial for normal physiological functions [2]. Arsenic is naturally present in water, soils, rocks, and living organisms; however, anthropogenic activities such as mining, smelting, and the use of arsenic-containing pesticides and wood preservatives have significantly contributed to its widespread distribution and increased levels in the environment [3]. Chronic exposure to arsenic can lead to a range of adverse health effects, including various cancers (skin, lung, bladder, and kidney), skin lesions, cardiovascular diseases, neurotoxicity, and diabetes [4]. Alarmingly, arsenic contamination in drinking water affects millions globally, particularly in regions with high natural arsenic levels in groundwater, such as parts of Asia, South America, and North America [5]. Given its high toxicity and widespread presence, regular monitoring and removal of arsenic from various sources, including natural waters, are imperative. The World Health Organization (WHO) has set a stringent limit of 10 ng/mL (or 10 parts per billion) for total arsenic in drinking water, necessitating the use of highly sensitive and accurate analytical techniques [6]. Several analytical methods have been employed for trace arsenic determination, each with advantages and limitations. While relatively simple and inexpensive, colorimetric methods often lack sensitivity and selectivity [7]. Atomic absorption spectrometry (AAS) and hydride generation systems combined with AAS offer improved sensitivity but can be time-consuming and require experienced operators [8]. Inductively coupled plasma mass spectrometry (ICP-MS) and atomic fluorescence spectrometry provide exceptional sensitivity and multi-element analysis capabilities but are often costly and require complex instrumentation [9]. In recent years, nanoparticle-based sensors have emerged as

*Corresponding author e-mail: Omniafahmey23@hotmail.com (Omnia M. Fahmy).
Received date 04 July 2024; revised date 03 August 2024; accepted date 06 August 2024
DOI: 10.21608/EJCHEM.2024.301718.9950

promising tools for predicting heavy metal pollution accumulation, translocation, and eco-toxicological impacts [10]. Among these, the nanoparticle-based Quartz Crystal Microbalance (QCM) sensor has gained significant attention due to its advantages: affordability, selectivity, sensitivity, rapid response time, and potential for miniaturization and portability [11]. The QCM sensor operates on the principle of a piezoelectric effect, where a quartz crystal oscillates at a specific frequency when an alternating electric field is applied. When a target analyte interacts with the sensor surface, the mass change causes a shift in the oscillation frequency, which can be correlated to the analyte concentration. By functionalizing the sensor surface with specific nanoparticles or receptors, the QCM sensor can be tailored for selective and sensitive detection of various analytes, including heavy metals like arsenic [12].

Consequently, there is a pressing need for a swift, dependable, and highly sensitive sensor for arsenic detection capable of meeting the stringent regulatory limits and addressing the widespread contamination issues. Our current research endeavors focus on developing a single analytical sensor capable of detecting heavy metals like arsenic with high sensitivity, selectivity, and rapid response times. Arsenic contamination in groundwater and its associated health risks have become a global concern, affecting millions worldwide. The contamination can originate from natural geological processes and anthropogenic activities [13]. In several regions, notably in parts of Asia and South America, arsenic naturally occurs in aquifers due to the weathering of arsenic-bearing rocks and minerals. The release of arsenic into groundwater is influenced by various factors, including geochemical conditions, pH, redox potential, and the presence of microorganisms [14].

Anthropogenic sources of arsenic contamination include mining activities, industrial processes (such as smelting, coal combustion, and semiconductor manufacturing), agricultural practices (such as the use of arsenic-based pesticides and wood preservatives), and improper waste disposal [15]. Industrial effluents and wastewater discharge can introduce significant amounts of arsenic into water bodies, posing risks to human health and the environment [16]. In densely populated areas with high groundwater extraction rates, lowering water tables can mobilize naturally occurring arsenic from sediments, exacerbating the contamination problem [17].

Climate change and associated changes in precipitation patterns and groundwater recharge rates can further impact the distribution and mobility of arsenic in aquifers [18]. Arsenic contamination in drinking water has become a public health crisis in many regions, particularly in developing countries where access to safe drinking water is limited, and resources for water treatment are scarce [19]. Long-term exposure to arsenic-contaminated water has been linked to various health issues, including skin lesions, cardiovascular diseases, neurological disorders, and various types of cancer [20]. Addressing arsenic contamination requires a multi-faceted approach involving monitoring, remediation, and the development of cost-effective and sensitive detection techniques. Continuous monitoring of arsenic levels in water sources is crucial for identifying contaminated areas and assessing the effectiveness of remediation efforts [21]. While accurate, conventional analytical techniques can be time-consuming and expensive and require specialized laboratory facilities, which may not be readily available in resource-limited settings [22]. Developing nanoparticle-based sensors, such as the QCM sensor functionalized with specific nanoparticles or receptors, offers a promising solution for on-site, rapid, and cost-effective arsenic detection [23]. These sensors can potentially overcome the limitations of traditional analytical methods and provide real-time monitoring capabilities, enabling timely intervention and remediation efforts [24]. By addressing the pressing need for a swift, dependable, and susceptible arsenic sensor, our research aims to contribute to the global effort to mitigate the risks associated with arsenic contamination and improve access to safe drinking water for communities worldwide [25].

This study presents the development of a novel nano-structured hydrazinyl Schiff base Co(II) complex-functionalized Quartz Crystal Microbalance (QCM) sensor. The unique aspect of our research lies in the synthesis and comprehensive characterization of this complex, which exhibits exceptional colloidal stability, high surface area, and favorable hydrophobic properties. This work addresses the critical need for a rapid, reliable, and highly sensitive method for detecting trace levels of arsenic in aqueous systems. By integrating this novel nanostructure onto a QCM platform, we demonstrate its potential for environmental sensing, contributing significantly to water quality monitoring and public health protection.

2. Experimental Procedures and Methodology

2.1. Materials and Solutions

In this research study, high-purity chemicals were employed throughout the experimental procedures. The critical materials utilized included 1-hydrazinylphthalazine (obtained from Merck), 1-(2H-benzo[d][1,2,3]triazol-2-yl)propan-2-one (purchased from Sigma-Aldrich), and cobalt(II) chloride hexahydrate ($CoCl_2.6H_2O$, sourced from BDH). For the preparation of solutions and as a reaction medium, absolute ethanol of spectroscopic grade purity was procured from BDH. Bid stilled water, obtained from glass distillation apparatuses, was consistently used for all aqueous solution preparations. It is important to note that all chemicals and reagents employed in this study were of high purity and used as received from the suppliers without further purification or treatment steps. Using high-quality materials and solvents is crucial in ensuring the

reproducibility and accuracy of the experimental results and the successful synthesis and characterization of the desired compounds and nanostructures.

2.2. Instrumentation

The Cairo University in Egypt investigation used a comprehensive analytical approach to characterize various materials. Multiple scientific instruments and techniques were employed to analyze the intrinsic properties and features of the substances studied. Mass spectra were acquired using an MS-5988 GS-MS instrument (Hewlett-Packard) with electron ionization at 70 eV. UV-Vis spectra within the 200 to 700 nm range were recorded using a PerkinElmer spectrophotometer.

The Microanalytical Center at Cairo University conducted antimicrobial research, while cytotoxicity studies were conducted at the National Cancer Institute and Cairo University. Microanalysis for carbon, hydrogen, and nitrogen content was performed with a CHNS-932 (LECO) Vario Elemental analyzer. Melting points were determined using a TriForce XMTD-3000 apparatus. FT-IR spectra (4000 to 400 cm^{-1}) were obtained using a Perkin-Elmer 1650 spectrometer with KBr disks. The molar conductance of solid complex solutions in ethanol (10^{-3} M) was measured with a Jenway 4010 conductivity meter. The surface charge and particle size of hydrazinyl Co(II) complex nanoparticles were determined using a NanoSight NS500 instrument (Malvern Panalytical). BET surface area and pore volume were measured with a Quanta Chrome Nova Touch 4L analyzer, following degassing at 65°C for 1.25 hours. Atomic Force Microscopy (AFM) used an Oxford Jupiter XR AFM model, with samples prepared by sonication using an ultrasonic probe sonicator (UP400S, Hielscher).

Thin film synthesis was performed with a Spain coater instrument (Laurell-650Sz) under vacuum conditions. AFM images and roughness profiles were obtained at 47 nm x 47 nm with a gold tip in contact mode. Wettability was assessed using a Biolin Scientific contact angle analyzer (model T200) under sessile drop conditions. QCM-based hydrazinyl Co(II) complex nanosensors were established using an AT-cut quartz crystal chip with a gold electrode (Q-Sense, Shenzhen). The sensor was cleaned with an ammonia, H_2O_2, double-distilled water solution, then air-dried. Baseline QCM measurements were taken with double-distilled water before introducing arsenic solutions (0.1, 0.5, and 1 ppm) at a controlled flow rate.

2.3. QCM-Monitoring of Arsenic Ions

The study used a QCM system to monitor arsenic ions with QCM-based hydrazinyl Co(II) complex nanosensors. Measurements were conducted by applying a 1 ppm arsenic solution onto the nanosensor surface under different conditions—temperatures (25°C, 35°C, and 45°C), arsenic concentrations (0.1, 0.5, 1 ppm), and pH levels (4, 7, 10). The process involved repeated arsenic solution injection until QCM signal stabilization, indicating equilibrium in the binding interaction, followed by a rinse with double-distilled water to remove unbound particles. This method evaluated the nanosensors' effectiveness in detecting arsenic in various environmental settings by achieving precise measurements and equilibrium in binding interactions.

2.4. Synthesis of the studied compounds

2.4.1. Synthesis of Schiff Base Ligand (L)

Following our previous research [26] and the protocol in Reference [27], we synthesized a novel Schiff base ligand through a condensation reaction between 1-hydrazinylphthalazine and 1-(2H-benzo[d][1,2,3]triazol-2-yl)propan-2-one. Initially, 1-hydrazinylphthalazine (0.4 g, 2.48 mmol) was dissolved in hot absolute ethanol (65°C). Separately, 1-(2H-benzo[d][1,2,3]triazol-2-yl)propan-2-one (0.436 g, 2.48 mmol) was dissolved in hot ethanol. These solutions were combined in a 1:1 molar ratio and refluxed for six hours, resulting in the formation of a reddish-brown solid. This precipitate was filtered, washed, and recrystallized from ethanol, yielding the pure Schiff base ligand with an 81% yield (Fig 1).

2.4.2. Synthesis of Hydrazinyl Co(II) Complex and its Nanostructure

The synthesis of the nano cobalt complex involved a multi-step procedure. First, an ethanolic solution of the Schiff base ligand (0.6 g, 1.88 mmol) was dissolved in hot ethanol at 65°C. Cobalt (II) chloride ($CoCl_2$, 1.88 mmol) was dissolved in 20 mL of absolute ethanol in a separate container. The two solutions were combined and refluxed with continuous stirring for five hours, forming the cobalt(II) complex, precipitating as a solid (Fig 1). This solid was isolated by filtration, thoroughly washed, and dried under a vacuum with anhydrous calcium chloride as a desiccant [28]. Recrystallization yielded the pure cobalt(II) complex. A color change from reddish-brown to yellowish-green was observed during the synthesis, likely due to the cobalt(II) ion's coordination with the Schiff base ligand. The synthesized cobalt(II) complex was further treated with ultrasonic probe sonication for 10 minutes [29, 30], promoting the breakdown of larger particles into nanoscale structures and facilitating the formation of nanostructured materials.

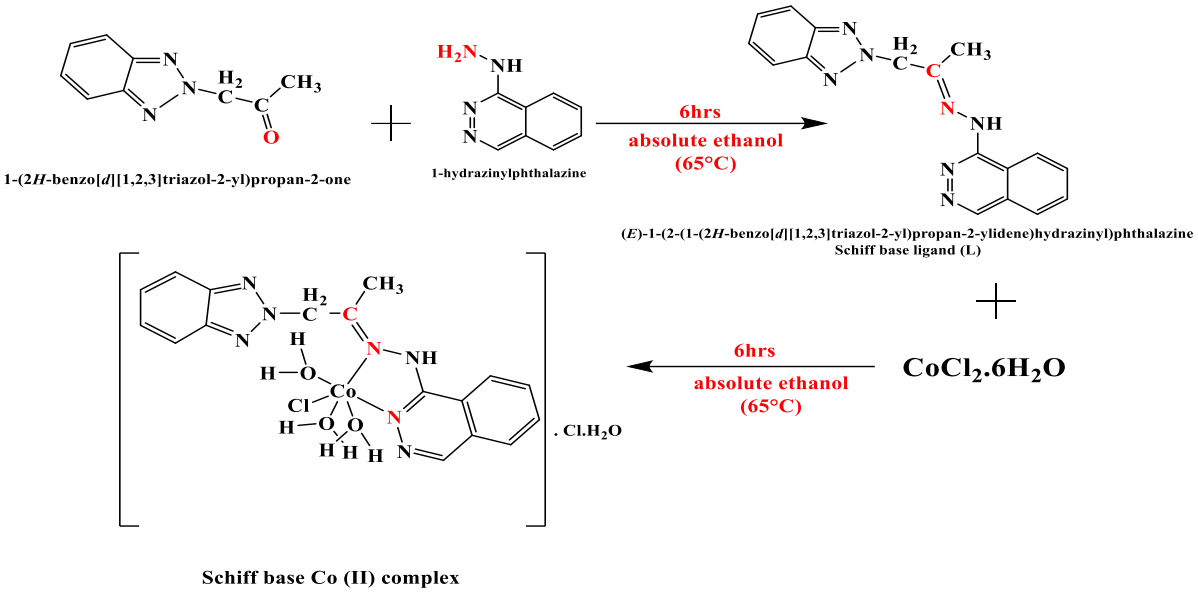

Fig 1. The structure of the Hydrazinyl Schiff Base and its Co(II) Complex formation reaction.

3. Result and Discussion

3.1.Characterization of Hydrazinyl Co(II) Complex

3.1.1. Spectroscopic and Thermogravimetric Characterization

The Cobalt complex stands out due to its distinct chemical composition and noteworthy biological attributes [31]. This complex exhibit stability in air and readily dissolves in polar organic solvents such as dimethylformamide (DMF) and dimethyl sulfoxide (DMSO). However, it demonstrates limited solubility in water. Elemental analysis affirms a 1:1 metal-to-ligand ratio for the complex. In DMSO concentration of 10^{-3} M) at 25 °C, its molar conductivity (Λm) registers at 62 Ω^{-1} mol^{-1} cm^2, indicating its electrolytic nature [27].The newly synthesized Schiff base cobalt complex exhibited favorable characteristics with a yield of 84%, a melting point of 249°C, and presented as a dark brown solid. Based on the provided information, the elemental analysis results obtained experimentally [C, 39.02%; H, 4.16%; Co, 11.05%; N, 18.57%] are in agreement with the calculated values [C, 39.32%; H, 4.46%; Co, 11.35%; N, 18.88%] for the proposed chemical compound $[Co(L)Cl(H_2O)_3]\cdot Cl\cdot H_2O$, where L represents the ligand with the molecular formula $\mathbf{C_{17}H_{23}Cl_2CoN_7O_4}$.

The close match between the calculated and experimental percentages of carbon (C), hydrogen (H), chlorine (Cl), cobalt (Co), and nitrogen (N) confirms the 1:1 metal-to-ligand ratio. It validates the composition of the complex [27, 32]. The EI-MS technique was used in this work to corroborate the mass of the Cobalt complex by examining the intense molecular ion peaks in the spectra shown at m/z = 521.20 $[M+2]^+$. The coordination mechanism between the ligand and the cobalt center is revealed through a comparative analysis of the infrared spectra of the ligand and the cobalt complex. Notably, the azomethine group and N-phthalazine in the ligand exhibit a robust band at 1627 and 1574 cm^{-1}, respectively, which shift to 1613 and 1545 cm^{-1} in the complex [33, 34].

This shift signifies coordination through the two nitrogen atoms. Additional nonligand bands at 463 cm^{-1} and 565 cm^{-1} correspond to υ(M−N) and υ(M−O) coordinated water, respectively [35-37]. In the IR spectra of the ligand, the peaks corresponding to Triazol ring stretching and (N-N) triazole were revealed at 1563 and 1089 cm^{-1}, respectively [26, 38–39]. The triazole did not bind to the Cobalt metal cation, as shown by the unchanged band of the ν(N-N) mode at 1088 cm^{-1}in the IR spectra of the Cobalt complex [38, 39].

Based on this data, the proposed formula for the Cobalt complex is $\mathbf{[Co(L)Cl(H_2O)_3]\cdot Cl\cdot H_2O}$. The UV-Vis spectrum of the Cobalt complex reveals distinctive bands at 260 nm and 339 nm, indicative of π–π* and n–π* intramolecular transitions, respectively [27]. Regarding biological activity, the antibacterial and antifungal properties of the Cobalt complex were evaluated using the disc diffusion method [40, 41]. The study utilized Thermal Gravimetric Analysis (TGA) to assess the synthesized metal complexes' thermal resilience and distinguish between water molecules existing as hydrated or coordinated within their structures. Analysis through TG and DTG was conducted on the Schiff base ligand metal complexes,

examining their behavior across a temperature spectrum from ambient conditions to 800°C [27, 28]. The thermal analysis of the **$[Co(L)Cl(H_2O)_3]\cdot Cl\cdot H_2O$** complex exhibited three decomposition steps. The initial step, between 35-105°C with a peak at 93.8°C, led to the loss of hydrated water molecules, estimating a mass loss of 3.08% (calculated = 3.46%).

The subsequent step, between 105-245°C with a peak at 277.11°C and 313.6, involved the loss of **$C_7H_{12}ClN_3O_2$** with an estimated mass loss of 39.07% (calculated = 39.59%). The final step, between 345–800°C with a peak at 516.7 and 623.27°C, related to the loss of **$C_{10}H_9ClN_4$**with an estimated mass loss of 42.06% (calculated = 42.49%),leaving behind cobalt oxide (CoO) as the decomposition product.

3.1.2. Biological Applications: Antimicrobial Efficacy

Table 1 shows the antimicrobial activity data, represented by the zone of inhibition (in mm), of the hydrazinyl Schiff base ligand (**L**), the hydrazinyl Co(II) complex, and standard antibiotics against various microorganisms. By comparing the antimicrobial activity of the hydrazinyl Schiff base ligand (L) and its corresponding hydrazinyl Co(II) complex (Table 1), it is evident that the complexation with the Co(II) ion enhances the antimicrobial activity in most cases [32, 37, 41]. Against Gram-negative bacteria, the hydrazinyl Co(II) complex exhibits significantly higher antimicrobial activity than the free hydrazinyl Schiff base ligand (L). For instance, against Escherichia coli (ATCC:10536), the hydrazinyl Co(II) complex shows a zone of inhibition of 23±0.7 mm, which is substantially higher than the free ligand (10.3±0.6 mm) and comparable to the standard antibiotic gentamicin (27.0±1.0 mm).

Similarly, against Salmonella enterica (ATCC: 14028), the hydrazinyl Co(II) complex demonstrates a higher zone of inhibition (19.8±1.0 mm) compared to the hydrazinyl Schiff base ligand (L) (9.0±1.0 mm), and its activity is slightly higher than the standard antibiotic gentamicin (18.3±0.6 mm). The hydrazinyl Co(II) complex also exhibits enhanced antimicrobial activity against Gram-positive bacteria compared to the free hydrazinyl Schiff base ligand (L). Against Staphylococcus aureus (ATCC:13565), the hydrazinyl Co(II) complex shows a higher zone of inhibition (23.7±1.0 mm) than the free ligand (10.0±1.0 mm), and its activity is slightly higher than the standard antibiotic ampicillin (22.0±1.0 mm). For Streptococcus mutans (ATCC:25175), the hydrazinyl Co(II) complex displays a higher zone of inhibition (18.9±0.3 mm) compared to the hydrazinyl Schiff base ligand (L) (15.3±0.6 mm), but slightly lower than the standard antibiotic ampicillin (20.3±0.6 mm). Regarding antifungal activity, the hydrazinyl Co(II) complex exhibits higher antimicrobial activity against Candida albicans (ATCC:10231) compared to the free hydrazinyl Schiff base ligand (L), with a zone of inhibition of 24±0.6 mm for the complex and 16.7±0.6 mm for the free ligand. The activity of the hydrazinyl Co(II) complex is higher than the standard antifungal agent nystatin (21.0±1.0 mm). However, against Aspergillus nigar (ATCC:16404), the hydrazinyl Co(II) complex shows a slightly lower zone of inhibition (21±0.6 mm) compared to the hydrazinyl Schiff base ligand (L) (20.3±0.6 mm). Still, its activity is comparable to the standard antifungal agent nystatin (19.3±0.6 mm).

The enhanced antimicrobial activity of the hydrazinyl Co(II) complex can be attributed to the presence of the Co(II) ion, which can interact with biomolecules and potentially disrupt cellular processes. The chelation of the hydrazinyl Schiff base ligand with the Co(II) ion can also modify the lipophilicity and solubility properties, facilitating better penetration into microbial cells and improving antimicrobial efficacy. The hydrazinyl Co(II) complex is more active than the hydrazinyl Schiff base ligand due to the chelation effect, structural modifications, redox properties, and altered solubility imparted by the complexation with the Co(II) ion. Our studies collectively demonstrate that the complexation of Schiff base ligands with metal ions consistently enhances antimicrobial activity. Our research shows the Co(II) complex significantly outperforms the free hydrazinyl Schiff base ligand against various microorganisms, often matching or exceeding standard antibiotics. This aligns with Abdel-Rahman et al.'s (2023) findings, where their metal complexes, especially the Mn(II) complex, exhibited superior antimicrobial activity compared to the free ligands [37].

Similarly, El-Sherif et al., in two separate studies, observed enhanced efficacy of their metal complexes, particularly Zn(II) and Cd(II) complexes, against a range of pathogens. Across all studies, the improved activity is attributed to increased lipophilicity, metal ion interactions with cellular components, and altered physicochemical properties due to complexation [32,41].

The enhanced antimicrobial activity of your hydrazinyl Co(II) complex aligns with several mechanisms proposed in recent literature. Despite variations in specific metals and ligands used, the consistent enhancement of antimicrobial properties upon complexation highlights the potential of Schiff base metal complexes as promising candidates for new antimicrobial agents.

Table 1. Antimicrobial Activity (Zone of Inhibition in mm) of Schiff Base Ligand (L), hydrazinyl Co(II) complex, and Standard Antibiotics against Various Microorganisms

Sample / Microorganism	Schiff base Ligand (L)	hydrazinyl Co(II) complex	Standard antibiotic
Gram-negative bacteria			**Gentamicin**
Escherichia coli (ATCC:10536)	10.3±0.6	23±0.7	27.0±1.0
Salmonella enterica (ATCC: 14028)	9.0±1.0	19.8±1.0	18.3±0.6
Gram-positive bacteria			**Ampicillin**
Staphylococcus aureus (ATCC:13565)	10.0±1.0	23.7±1.0	22.0±1.0
Streptococcus mutans (ATCC:25175)	15.3±0.6	18.9±0.3	20.3±0.6
Fungi			**Nystatin**
Candida albicans (ATCC:10231)	16.7±0.6	24±0.6	21.0±1.0
Aspergillus Nigar (ATCC:16404)	20.3±0.6	21±0.6	19.3±0.6

3.2. Characterization of Nano-Hydrazinyl Co(II) Complex

3.2.1. Textural Characterization of Hydrazinyl Co(II) Complex Nanoparticles by SEM and AFM

Scanning electron microscopy (SEM) is a well-known and practical method for determining the surface morphology of produced hydrazinyl Co(II) complex nanoparticles [42, 43]. The SEM images in Fig 2 indicate the excellent dispersity achieved for these nanoparticles. The images reveal that the particles show a particulate or granular morphology, with small spherical or near-spherical particles clustered together and showing no apparent signs of aggregation or agglomeration. Furthermore, the particle diameters are consistently below 100 nm, ranging in size from 34.11 to 61.95 nm. Atomic Force Microscopy (AFM) images [44, 45], as depicted in Figure 3, vividly illustrate a fibrous morphology for the hydrazinyl Co(II) complex nanoparticles. These images revealed no observable signs of aggregation or agglomeration. The particle size, extrapolated from the AFM images, was determined to be less than 54 nm. The complementary information provided by SEM and AFM analyses allowed for a comprehensive characterization of the textural properties and morphology of the hydrazinyl Co(II) complex nanoparticles. The SEM images confirmed the successful synthesis of well-dispersed, spherical nanoparticles with diameters below 100 nm, while the AFM images revealed a fibrous nanostructure with particle sizes below 52 nm. These findings are critical in understanding the nanoparticles' structural features and potential implications for various applications, such as sensing and catalysis.

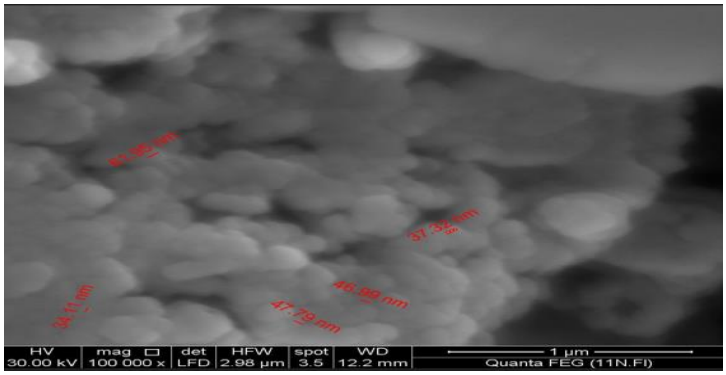

Fig 2. SEM Imaging Reveals Well-Dispersed Spherical Hydrazinyl Co(II) Complex Nanoparticles with Sub-100 nm Diameters.

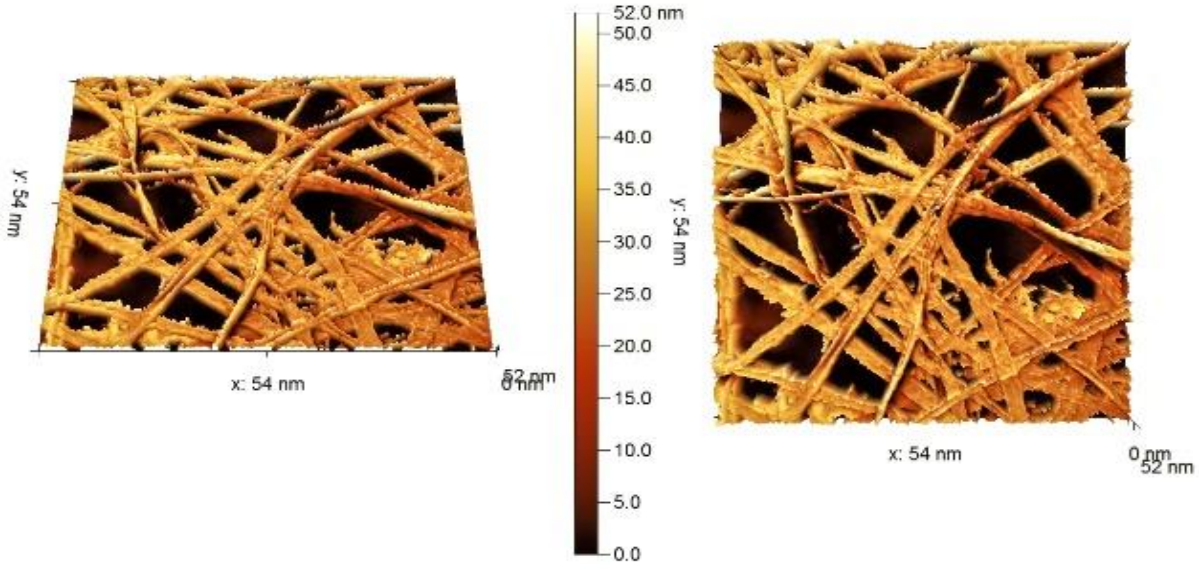

(A) **(B)**

Fig 3. (A) Depict the 3D Atomic Force Microscopy (AFM) on the left, and **(B)** Depict the 3D Two-Dimensional Atomic Force Microscopy (2DAFM) on the right for Cd (II) complex nanoparticles.

3.2.2. Dynamic Light Scattering (DLS) and Zeta Potential Analysis

The particle size assessment of the hydrazinyl Co(II) complex nanoparticles was carried out using the dynamic light scattering (DLS) technique [46, 47], as depicted in Figure 4. The DLS analysis revealed that the average particle size of the hydrazinyl Co(II) complex nanoparticles was 68.061 nm. The results showed an unimodal size distribution with a low polydispersity index, indicating a remarkably high colloidal stability within the suspension. Figures (4 and 5) illustrate the particle size distribution and zeta potential outcomes for the hydrazinyl Co(II) complex nanoparticles. Notably, the measured zeta potential was -32.674 Mv (Fig 5), suggesting a uniform dispersion of nanoparticles. The zeta potential, a critical parameter in evaluating the physicochemical stability of colloidal systems during storage, reflects the system's overall stability [48, 49]. A higher absolute value of the zeta potential corresponds to better system stability. The results presented here unequivocally highlight the exceptional stability of the hydrazinyl Co(II) complex nanoparticles. The DLS analysis provided quantitative information about the particle size distribution and confirmed the nanoscale dimensions of the synthesized hydrazinyl Co(II) complex particles. The low polydispersity index indicated a narrow size distribution and high monodispersity, desirable characteristics for many applications. Furthermore, the zeta potential analysis revealed the presence of surface charges on the nanoparticles, contributing to their colloidal stability through electrostatic repulsion forces. The high absolute value of the zeta potential (-32.674 mV) suggested excellent stability and minimal tendency for aggregation or agglomeration. Together, these analyses provided valuable insights into the size, dispersity, and stability of the hydrazinyl Co(II) complex nanoparticles, essential for their successful implementation in various applications.

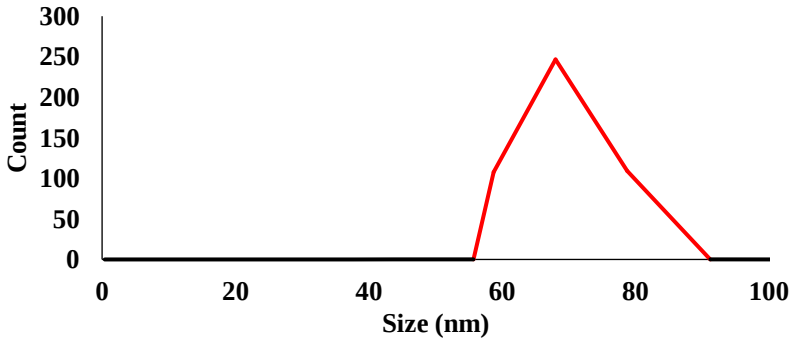

Fig 4. Dynamic Light Scattering (DLS) Analysis of Hydrazinyl Co(II) Complex Nanoparticles Showing Average Particle Size and Size Distribution

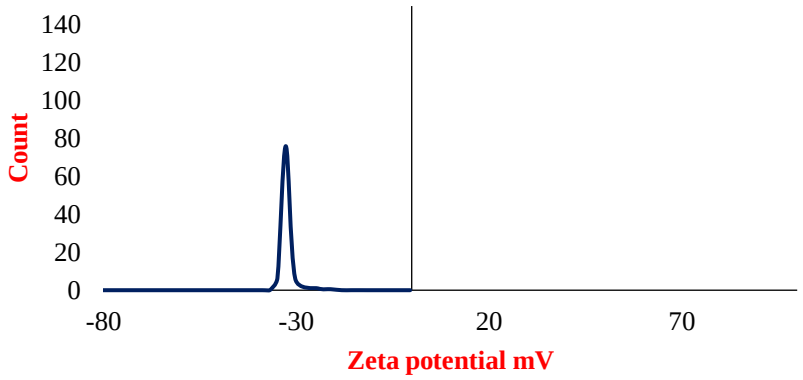

Fig 5. Zeta Potential of Hydrazinyl Co(II) Complex Nanoparticles Indicating High Colloidal Stability

3.2.3. BET Surface Area and Pore Size Analysis

The Brunauer–Emmett–Teller (BET) method is a powerful technique for characterizing nanomaterials, providing valuable insights into their surface area and porosity. In the case of the hydrazinyl Co(II) complex nanoparticles, the application of BET adsorption isotherms played a crucial role in scrutinizing their surface area characteristics (Fig 6) [50, 51]. The nitrogen adsorption-desorption isotherms exhibited a characteristic type IV behavior, indicating the presence of hysteresis loops, confirming the macroporous nature of these nanoparticles. The BET analysis revealed a surface area of 93.5578 m^2/g for the hydrazinyl Co(II) complex nanoparticles. Additionally, the average particle radius was determined to be 14.575 nm, and the average pore size was found to be 3.18822 nm. The substantial surface area, as elucidated by the multipoint BET analysis, significantly enhances the capacity of these metal complex nanoparticles to adsorb arsenic ions from aqueous environments. This remarkable surface area can be attributed to the unique fibrous morphology of the nanoparticles, as evidenced by the AFM analysis, which revealed a fiber-like structure with a diameter of approximately 52 nm. The macroporous structural characteristics, stemming from the fibrous morphology, play a pivotal role in augmenting the efficacy of arsenic ion adsorption by these metal complex nanoparticles. The high surface area and macroporous nature provide abundant active sites and enhanced accessibility for arsenic ions to interact with the nanoparticle surface [52]. Furthermore, the fibrous morphology with a diameter of 52 nm contributes to the high surface area. It facilitates the adsorption process by providing a more significant number of binding sites and potential ion exchange channels along the length of the fibers. This unique fibrous architecture creates a highly conducive environment for efficient arsenic ion adsorption and subsequent removal from aqueous solutions [53, 54]. The macroporous structure, substantial surface area, and fibrous morphology with a favorable fiber diameter make these complex metal nanoparticles highly attractive for arsenic ion adsorption and remediation applications. The synergistic effect of these characteristics enhances the nanoparticles' adsorption capacity, selectivity, and kinetics, ultimately leading to improved arsenic ion removal efficacy.

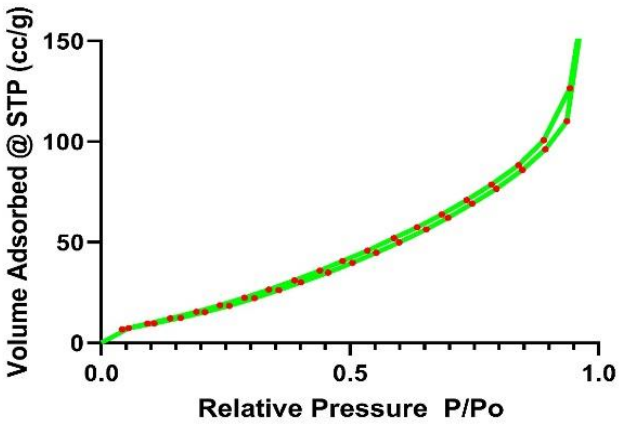

Fig 6. BET Adsorption Isotherms Analysis of Hydrazinyl Co(II) Complex Nanoparticles for Surface Area Characterization

3.2.4. Contact Angle, Hydrophobicity, and Toxicity of Hydrazinyl Co(II) Complex Nanoparticles

The hydrophobic nature of the hydrazinyl Co(II) complex nanoparticles is evident from the considerable water contact angle measured at 117.3° (Fig 7). This inherent hydrophobic characteristic enhances the suitability of these nanoparticles for practical sensing applications in aqueous environments [55-57]. In developing eco-friendly nanoparticle-based sensors, ensuring the material's non-toxicity is essential. A thorough evaluation of the cytotoxicity of the hydrazinyl Co(II) complex nanoparticles resulted in a reassuring IC_{50} value of 653 µg/ml (Fig 8) [58, 59]. The notably high IC_{50} value provides confidence in the potential utilization of these nanoparticles as sensors in water-related applications, emphasizing their safety and environmental compatibility. The hydrophobic nature of the nanoparticles, as indicated by the high-water contact angle, is advantageous for sensing applications in aqueous environments. This property facilitates the interaction and adsorption of target analytes onto the nanoparticle surface, enhancing the sensitivity and selectivity of the sensing system. Furthermore, the low cytotoxicity of the hydrazinyl Co(II) complex nanoparticles, as demonstrated by the high IC_{50} value, is a crucial consideration for their practical implementation. It ensures that the nanoparticles pose minimal risk to biological systems and the environment, making them suitable for water quality monitoring and remediation applications. The hydrazinyl Co(II) complex nanoparticles offer a promising platform for developing eco-friendly and efficient sensing systems for detecting and monitoring various analytes in aqueous environments by combining the hydrophobic nature and low cytotoxicity.

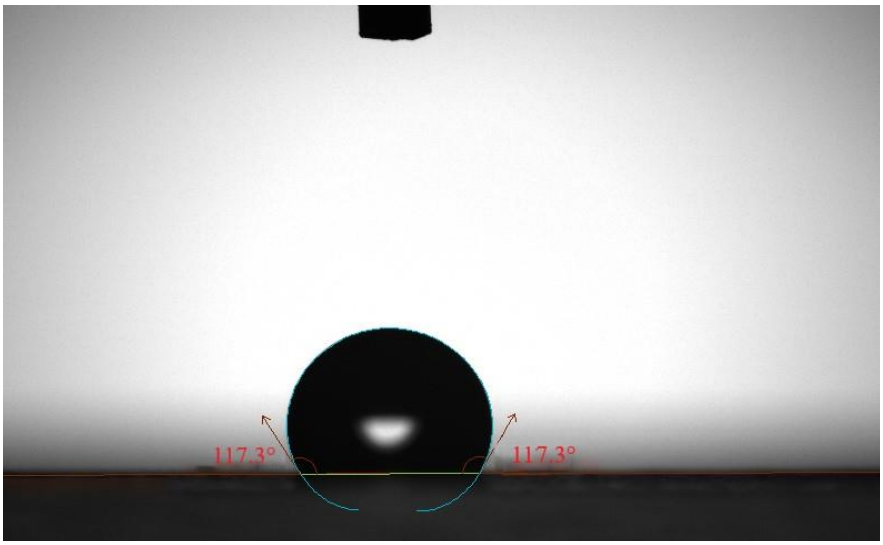

Fig 7. Water Contact Angle Measurement of Hydrazinyl Co(II) Complex Nanoparticles Demonstrating Hydrophobicity

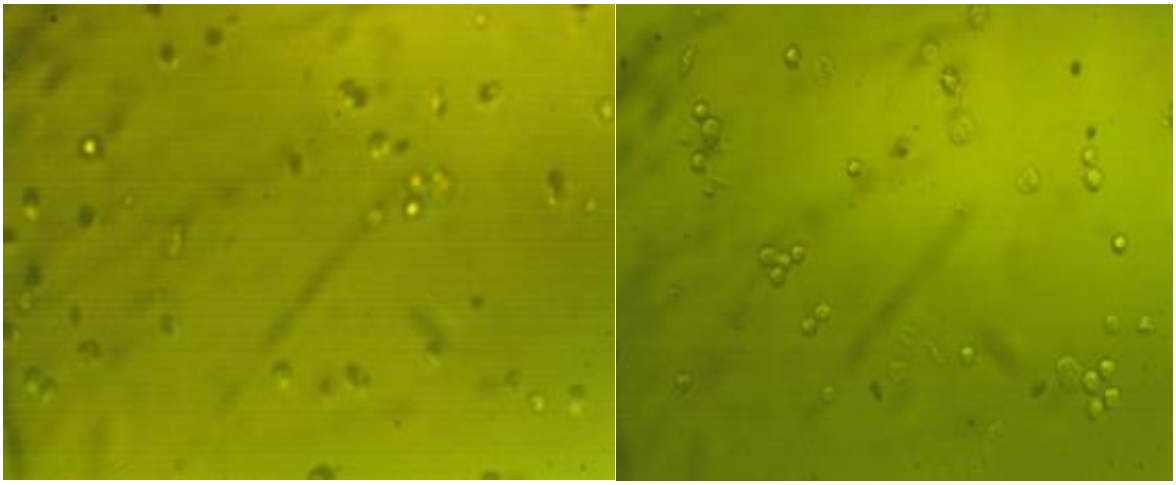

Fig 8. Cytotoxicity Evaluation of Hydrazinyl Co(II) Complex Nanoparticles Indicating High IC_{50} Value for Safe Use in Water-Related Applications

3.2.5. Arsenic Ion Monitoring Using QCM-Based Hydrazinyl Co(II) Complex Nanosensors

A typical experiment utilizing a Quartz Crystal Microbalance (QCM)-based hydrazinyl Co(II) complex nanosensor for detecting arsenic ions can be divided into four distinct stages, each revealing crucial information about the sensor's performance [27, 58]:

1. Baseline Stability: The sensor's frequency response is recorded in the initial stage, providing a stable baseline measurement. This step serves as a reference point for the subsequent stages.
2. Rapid Frequency Drop upon Arsenic Ion Binding: A sudden and significant decrease in frequency is observed as arsenic ions rapidly bind to the sensor's surface. This rapid change is attributed to the occupation of numerous vacant sites on the sensor's surface by arsenic ions.
3. Continued Adsorption of Arsenic Ions: As the experiment progresses, further adsorption of arsenic ion molecules takes place on the hydrazinyl Co(II) complex nanosensor's surface. This stage demonstrates the sensor's ability to capture additional arsenic ions.
4. Equilibrium State: Eventually, an equilibrium state is achieved in the adsorption process between the hydrazinyl Co(II) complex and arsenic ion molecules. The sensor's frequency shift stabilizes, indicating that the maximum capacity for arsenic ion adsorption has been reached.

Figure 9 accompanying this description visually illustrates the sensor's performance throughout these stages, showcasing its capacity to bind arsenic ions effectively. Once the frequency stabilizes again, it signifies the attainment of an equilibrium state in the adsorption of arsenic ions on the QCM-based hydrazinyl Co(II) complex nanosensor's surface [60, 61]. No noticeable changes in the sensor's frequency are observed at this fourth stage. This implies minimal mass loss has occurred, and any structural modifications to the nanosensor's surface are minor. Consequently, this reaffirms the sensor's effectiveness in detecting arsenic ions. The ability of the QCM-based hydrazinyl Co(II) complex nanosensor to undergo these distinct stages during the arsenic ion monitoring process demonstrates its sensitivity, selectivity, and reliability in detecting and quantifying arsenic contamination in aqueous environments.

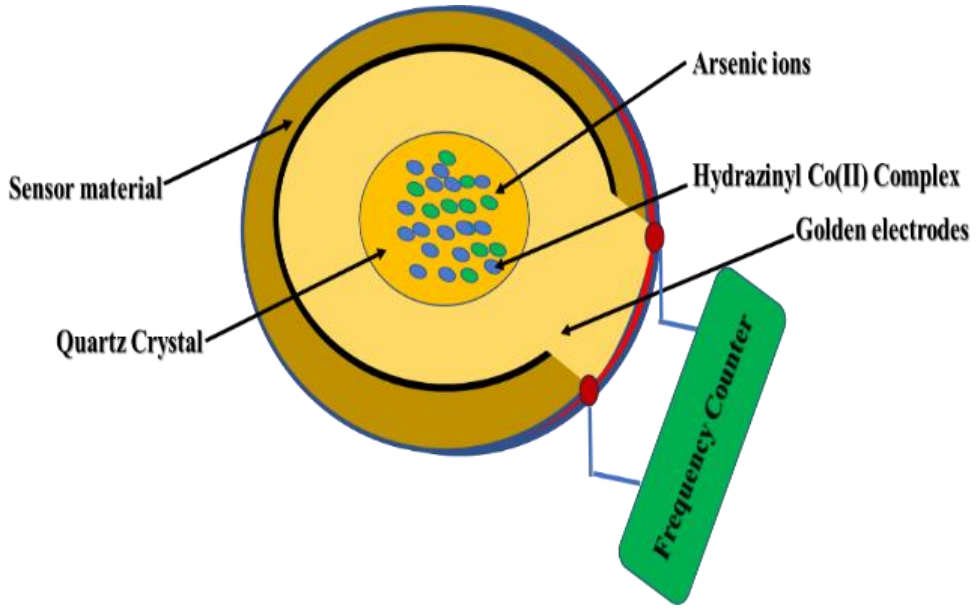

Fig 9. Arsenic Ion Monitoring Using QCM-Based Hydrazinyl Co(II) Complex Nanosensors

3.2.5.1. Proposed Sensing Mechanism of the QCM-Based Nano Hydrazinyl Co(II) Complex

Due to the lower electronegativity of arsenic ions compared to the nano hydrazinyl Co(II) sensor, dipole-dipole interactions are likely to arise. These can be complemented by π–π interactions between the aromatic hydrazinyl moieties of the complex and the arsenic ions. Nitrogen-containing heterocycles and other polar functional groups in the nano hydrazinyl Co(II) complex can increase negative charge density on the sensor's surface. Consequently, the QCM-based nano hydrazinyl Co(II) sensor exhibits an enhanced propensity to interact with arsenic ions, primarily through electrostatic attractions facilitated by the negatively charged surface, in conjunction with the π–π interactions between the aromatic hydrazinyl groups and the arsenic ions [27, 58].

3.2.5.2. Effect of Temperature

Chemical adsorption processes are significantly influenced by temperature, and the adsorption rate can be increased or decreased depending on the temperature conditions [62]. When the temperature rises, the arsenic ion molecules and the nano hydrazinyl Co(II) complex gain more kinetic energy, resulting in faster movement and a higher frequency of collisions between them. This can lead to an increased rate of adsorption. In adsorption, higher temperatures facilitate the diffusion of arsenic ion molecules through the boundary layer surrounding the nano hydrazinyl Co(II) complex adsorbent and within its porous structure. The enhanced kinetic energy of the molecules at elevated temperatures allows them to overcome potential energy barriers more readily and access the adsorption sites. Additionally, changing the temperature can influence the adsorption equilibrium capacity of the nano hydrazinyl Co(II) complex towards arsenic ions, potentially enhancing the overall adsorption performance. At higher temperatures like 45°C (green curve) (Fig 10), there is a much steeper initial drop in frequency than at lower temperatures. This rapid frequency decrease indicates a faster binding or mass-loading process on the sensor surface at elevated temperatures. The 35°C (red) and 25°C (blue) curves (Fig 10) also exhibit this pattern, with steeper initial frequency drops at higher temperatures, signifying accelerated binding/mass loading kinetics driven by the increased thermal energy. Moreover, the curves reach lower final frequency values at higher temperatures. This suggests higher temperatures enable greater overall mass binding or analyte capture on the sensor, resulting in more significant total frequency shifts. In summary, this data demonstrates that increasing the temperature enhances both the rate (from the initial slope) and the extent (from the final frequency shift) of the frequency change process, likely due to accelerated analyte binding/mass loading at higher thermal energies.

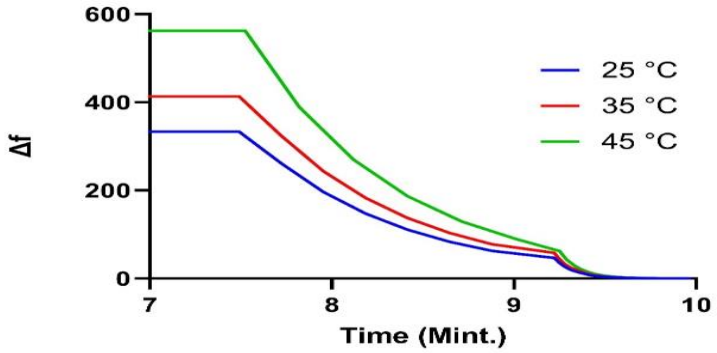

Fig 10. Temperature-Dependent Frequency Shift in Arsenic Ion Adsorption by Nano Hydrazinyl Co(II) Complex Sensor

3.2.5.3. Effect of pH on Arsenic Ion Adsorption by the Nano Hydrazinyl Co(II) Complex

The initial pH of the solution plays a crucial role in the adsorption of arsenic ions onto the nano hydrazinyl Co(II) complex due to its influence on the chemical speciation of arsenic ions and the ionization state of functional groups on the complex's surface [63, 64]. Figure 11 shows the change in frequency (Δf) over time for the nano hydrazinyl Co(II) complex-based sensor at different pH values: 4, 7, and 10. These curves illustrate the effect of pH on the adsorption of arsenic ions onto the sensor surface. At pH 4 (blue curve), the sensor exhibits a rapid and substantial initial decrease in frequency, indicating efficient adsorption of arsenic ions onto the sensor's surface. This behavior can be attributed to the protonation of functional groups on the nano hydrazinyl Co(II) complex, facilitating electrostatic interactions with the positively charged arsenic species and leading to enhanced adsorption. The initial frequency drop is less pronounced at pH 7 (red curve) compared to pH 4, suggesting a relatively lower adsorption capacity at this neutral pH value. This observation confirms that optimal adsorption often occurs within the slightly acidic pH range. In contrast, at neutral pH values, the adsorption may be reduced due to different arsenic species or changes in the sensor's surface chemistry. Notably, the frequency shift curve for pH 10 (green curve) exhibits a distinct behavior. Initially, a slight increase in frequency is observed, indicating a potential desorption or repulsion of species from the sensor's surface. This phenomenon can be attributed to the deprotonation of functional groups at high pH values, leading to electrostatic repulsion between the negatively charged sensor surface and the negatively charged arsenic species in the solution. Moreover, as the pH level is elevated, the leaching of arsenic becomes apparent, as mentioned in the provided text. This leaching effect results in a decreased rate of adsorption, consequently diminishing the removal capacity of arsenic ions, as visually depicted by the gradual decrease in frequency after the initial increase at pH 10. The observed behavior at high pH can be further expounded upon by considering the augmented presence of sodium ions (Na^+) in the solution, which is attributed to pH adjustments. These sodium ions can compete with the remaining arsenic ions for the available exchangeable sites on the sensor's surface, thereby hindering the adsorption of arsenic ions and contributing to the observed decrease in frequency shift [65]. In summary, the nano hydrazinyl Co(II) complex-based sensor exhibits optimal adsorption of arsenic ions under slightly acidic conditions (around pH 4). In contrast, adsorption is reduced at neutral pH and further diminished at high pH due to deprotonation, leaching, and competition from other ions.

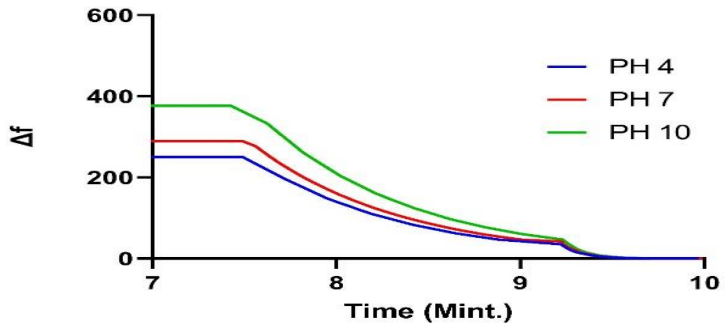

Fig 11. pH-Dependent Frequency Shift in Arsenic Ion Adsorption by Nano Hydrazinyl Co(II) Complex Sensor

3.2.5.4. Effect of Concentration

Figure 12 illustrates the effect of arsenic ion concentration on its detection by the hydrazinyl Co(II) complex over time. The three curves correspond to different concentrations of arsenic ions: 0.1 ppm (parts per million), 0.5 ppm, and 1 ppm. At the initial time (around 7 minutes), the absorbance values for all three concentrations are high, indicating a strong detection signal. The higher the concentration of arsenic ions, the higher the initial absorbance value. As time progresses, the absorbance values decrease for all three concentrations. This decrease can be attributed to the reaction between the hydrazinyl Co(II) complex and the arsenic ions, where the complex binds to or interacts with the arsenic ions, leading to a change in the absorbance signal. The concentration of arsenic ions influences the rate of decrease in absorbance. The curve for the highest concentration (1 ppm) shows a more gradual decrease compared to the curves for lower concentrations (0.5 ppm and 0.1 ppm). This can be explained by the fact that at higher concentrations, more arsenic ions are available to interact with the hydrazinyl Co(II) complex, resulting in a slower depletion of the complex and a more gradual decrease in absorbance [66]. The graph demonstrates that the hydrazinyl Co(II) complex is sensitive to different concentrations of arsenic ions, as evidenced by the distinct curves for each concentration. However, the detection limit of the complex may be lower than 0.1 ppm, as the curve for this concentration appears to approach a plateau around 9-10 minutes, indicating that the complex may have been consumed or saturated at this point. It is worth noting that the true information about the specific hydrazinyl Co(II) complex used and the experimental conditions would be required to provide a more detailed and accurate interpretation of the observed trends. Additionally, factors such as the stability of the complex, the reaction kinetics, and any potential interfering species could influence the detection process and the absorbance values over time.

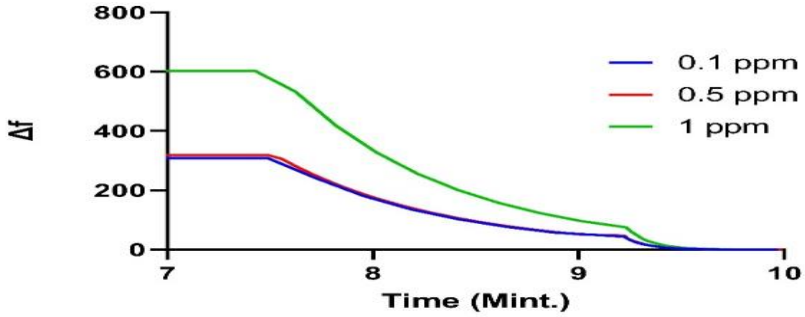

Fig 12. Effect of Arsenic Ion Concentration on Detection by Hydrazinyl Co(II) Complex

4. Conclusion

The development of this nanostructured hydrazinyl Schiff base Co(II) complex and its functionalization onto a quartz crystal microbalance (QCM) sensor represents a significant advancement for rapid and sensitive detection of arsenic in aqueous systems. The unique properties of these nanoparticles have been thoroughly investigated through comprehensive characterization using various analytical techniques like DLS, zeta potential, TEM, AFM, BET, contact angle, and cytotoxicity studies. The hydrazinyl Co(II) complex nanoparticles exhibit excellent colloidal stability, high surface area, fibrous morphology, and favorable hydrophobic nature, making them well-suited for sensing in aqueous environments. Their low cytotoxicity further enhances their suitability for environmental applications. By integrating these nanoparticles onto a QCM sensor platform, a highly sensitive and selective arsenic detection system has been developed. The QCM nanosensor

demonstrated the ability to detect arsenic down to 1 ppm concentration with a remarkable (7-8) minute response time. The distinct detection stages of rapid frequency drop, continued adsorption, and equilibrium state highlight the sensor's sensitivity, selectivity, and reliability. This innovative nanosensor addresses the critical need for rapid, reliable, and highly sensitive arsenic detection methods. It contributes significantly towards mitigating the risks of arsenic contamination and enabling access to safe drinking water globally. Successful development of this QCM nanosensor paves the way for further advancements in environmental sensing and water quality monitoring with potential applications across public health, environmental remediation, and industrial wastewater treatment sectors.

5. References

1. M. M. Hassan, Arsenic in Groundwater. Boca Raton: Taylor & Francis, a CRC title, part of the Taylor & Francis imprint, a member of the Taylor & Francis Group, the academic division of T&F Informa, plc, 2018.: CRC Press, 2018.
2. A. Vahidnia, G. B. van der Voet, and F. A. de Wolff, "Arsenic neurotoxicity — A review," Hum. Exp. Toxicol., vol. 26, no. 10, pp. 823–832, Oct. 2007.
3. P. Smedley and D. Kinniburgh, "A review of the source, behaviour and distribution of arsenic in natural waters," Appl. Geochemistry, vol. 17, no. 5, pp. 517–568, May 2002.
4. M. F. Naujokas et al., "The broad scope of health effects from chronic arsenic exposure: update on a worldwide public health problem," Environ. Health Perspect., vol. 121, no. 3, pp. 295–302, 2013.
5. P. Ravenscroft, H. Brammer, and K. Richards, Arsenic pollution: a global synthesis. John Wiley & Sons, 2011.
6. F. Edition, "Guidelines for drinking-water quality," WHO Chron., vol. 38, no. 4, pp. 104–108, 2011.
7. S. Bang, P. H. Viet, and K.-W. Kim, "Contamination of groundwater and risk assessment for arsenic exposure in Ha Nam province, Vietnam," Environ. Int., vol. 35, no. 3, pp. 466–472, 2009.
8. I. López-García and M. Hernández-Córdoba, "Atomic absorption spectrometry," Handb. Miner. Elem. food, pp. 189–217, 2015.
9. T. Van Acker, S. Theiner, E. Bolea-Fernandez, F. Vanhaecke, and G. Koellensperger, "Inductively coupled plasma mass spectrometry," Nat. Rev. Methods Prim., vol. 3, no. 1, p. 52, 2023.
10. A. Thakur and A. Kumar, "Ecotoxicity Analysis and Risk Assessment of Nanomaterials for the Environmental Remediation," in Macromolecular Symposia, Wiley Online Library, 2023, p. 2100438.
11. K. V Ragavan and S. Neethirajan, "Nanoparticles as biosensors for food quality and safety assessment," in Nanomaterials for food applications, Elsevier, 2019, pp. 147–202.
12. N. Alanazi, M. Almutairi, and A. N. Alodhayb, "A review of quartz crystal microbalance for chemical and biological sensing applications," Sens. Imaging, vol. 24, no. 1, p. 10, 2023.
13. E. Shaji, M. Santosh, K. V Sarath, P. Prakash, V. Deepchand, and B. V Divya, "Arsenic contamination of groundwater: A global synopsis with focus on the Indian Peninsula," Geosci. Front., vol. 12, no. 3, p. 101079, 2021.
14. S. J. S. Flora, "Arsenic: chemistry, occurrence, and exposure," in Handbook of arsenic toxicology, Elsevier, 2015, pp. 1–49.
15. P. Chowdhary, R. N. Bharagava, S. Mishra, and N. Khan, "Role of industries in water scarcity and its adverse effects on environment and human health," Environ. Concerns Sustain. Dev. Vol. 1 Air, Water Energy Resour., pp. 235–256, 2020.
16. I. Herath, M. Vithanage, J. Bundschuh, J. P. Maity, and P. Bhattacharya, "Natural arsenic in global groundwaters: distribution and geochemical triggers for mobilization," Curr. Pollut. Reports, vol. 2, pp. 68–89, 2016.
17. R. Bondu, V. Cloutier, E. Rosa, and M. Benzaazoua, "A review and evaluation of the impacts of climate change on geogenic arsenic in groundwater from fractured bedrock aquifers," Water, Air, Soil Pollut., vol. 227, pp. 1–14, 2016.
18. M. Barbieri et al., "Climate change and its effect on groundwater quality," Environ. Geochem. Health, vol. 45, no. 4, pp. 1133–1144, 2023.
19. S. Chowdhury, M. A. J. Mazumder, O. Al-Attas, and T. Husain, "Heavy metals in drinking water: occurrences, implications, and future needs in developing countries," Sci. Total Environ., vol. 569, pp. 476–488, 2016.
20. M. S. Rahaman et al., "Environmental arsenic exposure and its contribution to human diseases, toxicity mechanism and management," Environ. Pollut., vol. 289, p. 117940, 2021.
21. A. Bhat, K. Ravi, F. Tian, and B. Singh, "Arsenic Contamination Needs Serious Attention: An Opinion and Global Scenario," Pollutants, vol. 4, no. 2, pp. 196–211, 2024.
22. N. Jiang et al., "Low-cost optical assays for point-of-care diagnosis in resource-limited settings," ACS sensors, vol. 6, no. 6, pp. 2108–2124, 2021.
23. M. Bakhshpour, I. Göktürk, S. D. Gür, F. Yılmaz, and A. Denizli, "Sensor applications for detection in agricultural products, foods, and water," in Pesticides Bioremediation, Springer, 2022, pp. 311–352.
24. H. Abi Rizk, D. Bouveresse, J. Chamberland, and C. B. Y. Cordella, "Recent developments of e-sensing devices coupled to data processing techniques in food quality evaluation: a critical review.," Anal. Methods, 2023.
25. N. J. Raju, "Arsenic in the geo-environment: A review of sources, geochemical processes, toxicity and removal technologies," Environ. Res., vol. 203, p. 111782, 2022.

26. O. M. Fahmy, W. H. Mahmoud, R. M. El Nashar, and A. A. El-Sherif, "Nano Co (II) and Pd (II) Schiff base Complexes: Structural Characterization, Molecular docking, Antitumor proficiency and Biological evaluation," Egypt. J. Chem., vol. 66, no. 13, pp. 1373–1382, 2023.
27. M. S. Mansour, W. H. Mahmoud, and A. A. El-Sherif, "Manganese, Cobalt, and Cadmium Complexes of Quinazoline Schiff Base Ligand and Methionine: Synthesis, Characterization, DFT, Docking studies and biomedical application," Egypt. J. Chem., 2024.
28. M. S. A. Mansour, A. A. El-Sherif, W. H. Mahmoud, and abeer taha, "QCM-Based Nano Schiff base Quinazoline-methionine hybrid ligand complex with Cobalt (II) as a Fast Response Nanosensor for instantaneous Monitoring water pollutant Pb (II) Ions," Egypt. J. Chem., 2024.
29. M. A. Tarek, W. Mahmoud, M. A. E. Elmosallamy, and A. A. El-Sherif, "Cadmium detection with nickel complex nanoparticles sensor using QCM technique Mohamed T. Radwan 1, Walaa H. Mahmoud 1, Mohamed AF ElMosallamy 2 and Ahmed A. El-Sherif 1," Bull. Fac. Sci. Zagazig Univ., vol. 2024, no. 1, pp. 132–142, 2024.
30. W. H. Mahmoud, A. A. Fayek, A. Taha, and A. A. El-Sherif, "Synthesis, textural and thermal properties of Nano super hydrophobic cupper complex as QCM based dye sensor," Egypt. J. Chem., vol. 67, no. 4, pp. 485–494, 2024.
31. Y. Yildiz, "General aspects of the Cobalt Chemistry," Cobalt, vol. 1, 2017.
32. A. A. El-Sherif and T. M. A. Eldebss, "Synthesis, spectral characterization, solution equilibria, in vitro antibacterial and cytotoxic activities of Cu (II), Ni (II), Mn (II), Co (II) and Zn (II) complexes with Schiff base derived from 5-bromosalicylaldehyde and 2-aminomethylthiophene," Spectrochim. Acta Part A Mol. Biomol. Spectrosc., vol. 79, no. 5, pp. 1803–1814, 2011.
33. A. A. El-Sherif, A. Fetoh, Y. K. Abdulhamed, and G. M. A. El-Reash, "Synthesis, structural characterization, DFT studies and biological activity of Cu (II) and Ni (II) complexes of novel hydrazone," Inorganica Chim. Acta, vol. 480, pp. 1–15, 2018.
34. A. Hassan, B. H. Heakal, A. Younis, M. A. E.-M. Bedair, and M. M. A. Mohamed, "Synthesis of some triazole Schiff base derivatives and their metal complexes under microwave irradiation and evaluation of their corrosion inhibition and biological activity," Egypt. J. Chem., vol. 62, no. 9, pp. 1603–1624, 2019.
35. H. B. Schlegel, "Optimization of equilibrium geometries and transition structures," J. Comput. Chem., vol. 3, no. 2, pp. 214–218, 1982.
36. P. Tyagi, M. Tyagi, S. Agrawal, S. Chandra, H. Ojha, and M. Pathak, "Synthesis, characterization of 1,2,4-triazole Schiff base derived 3d-metal complexes: Induces cytotoxicity in HepG2, MCF-7 cell line, BSA binding fluorescence and DFT study," Spectrochim. Acta - Part A Mol. Biomol. Spectrosc., vol. 171, pp. 246–257, 2017.
37. L. H. Abdel-Rahman et al., "Novel Bromo and methoxy substituted Schiff base complexes of Mn(II), Fe(III), and Cr(III) for anticancer, antimicrobial, docking, and ADMET studies," Sci. Rep., vol. 13, no. 1, pp. 1–27, 2023.
38. N. F. Mahmoud, A. A. Abbas, and G. G. Mohamed, "Synthesis, characterization, antimicrobial, and MOE evaluation of nano 1, 2, 4-triazole-based Schiff base ligand with some d-block metal ions," Appl. Organomet. Chem., vol. 35, no. 6, p. e6219, 2021.
39. T. Matsuyama, K. Nakata, H. Hagiwara, and T. Udagawa, "Iron (II) Spin Crossover Complex with the 1, 2, 3-Triazole-Containing Linear Pentadentate Schiff-Base Ligand and the MeCN Monodentate Ligand," Crystals, vol. 9, no. 6, p. 276, 2019.
40. H. M. Fahmy, F. M. Abdel-Rahman, A. A. El-Sayed, and A. A. El-Sherif, "Study of novel bidentate heterocyclic amine-based metal complexes and their biological activities: cytotoxicity and antimicrobial activity evaluation," BMC Chem., vol. 17, no. 1, p. 78, 2023.
41. M. S. Aljahdali and A. A. El-Sherif, "Synthesis and biological evaluation of novel Zn (II) and Cd (II) Schiff base complexes as antimicrobial, antifungal, and antioxidant agents," Bioinorg. Chem. Appl., vol. 2020, pp. 1–17, 2020.
42. J. Rydz, A. Šišková, and A. Andicsová Eckstein, "Scanning electron microscopy and atomic force microscopy: topographic and dynamical surface studies of blends, composites, and hybrid functional materials for sustainable future," Adv. Mater. Sci. Eng., vol. 2019, 2019.
43. J. Rydz, A. Šišková, and A. Andicsová Eckstein, "Microscopic techniques in materials science: Current trends in the area of blends, composites, and hybrid materials," Advances in Materials Science and Engineering, vol. 2019. Hindawi, 2019.
44. Y. Z. Liu, X. R. Wu, Y. Sun, and W. L. Xie, "POSS dental nanocomposite resin: synthesis, shrinkage, double bond conversion, hardness, and resistance properties. Polymers-Basel 10 (4)." 2018.
45. G. K. Hassan, W. H. Mahmoud, A. Al-sayed, S. H. Ismail, A. A. El-Sherif, and S. M. Abd El Wahab, "Multi-functional of TiO2@ Ag core–shell nanostructure to prevent hydrogen sulfide formation during anaerobic digestion of sewage sludge with boosting of bio-CH4 production," Fuel, vol. 333, p. 126608, 2023.
46. E. Igarashi, Nanomedicines and nanoproducts: applications, disposition, and toxicology in the human body. CRC Press, 2018.
47. B. J. Berne and R. Pecora, Dynamic light scattering: with applications to chemistry, biology, and physics. Courier Corporation, 2000.

48. S. Bhattacharjee, "DLS and zeta potential–what they are and what they are not?," J. Control. release, vol. 235, pp. 337–351, 2016.
49. J. D. Clogston and A. K. Patri, "Zeta potential measurement," Charact. nanoparticles Intend. drug Deliv., pp. 63–70, 2011.
50. J. Rouquerol et al., "Recommendations for the characterization of porous solids (Technical Report)," Pure Appl. Chem., vol. 66, no. 8, pp. 1739–1758, 1994.
51. M. Thommes et al., "Physisorption of gases, with special reference to the evaluation of surface area and pore size distribution (IUPAC Technical Report)," Pure Appl. Chem., vol. 87, no. 9–10, pp. 1051–1069, 2015.
52. D. Mohan and C. U. Pittman Jr, "Arsenic removal from water/wastewater using adsorbents—a critical review," J. Hazard. Mater., vol. 142, no. 1–2, pp. 1–53, 2007.
53. A. Modak, P. Bhanja, M. Selvaraj, and A. Bhaumik, "Functionalized porous organic materials as efficient media for the adsorptive removal of Hg (II) ions," Environ. Sci. Nano, vol. 7, no. 10, pp. 2887–2923, 2020.
54. N. Hwang and A. R. Barron, "BET surface area analysis of nanoparticles," connexions Proj., pp. 1–11, 2011.
55. T. Du et al., "Multifunctional coatings of nickel-titanium implant toward promote osseointegration after operation of bone tumor and clinical application: a review," Front. Bioeng. Biotechnol., vol. 12, p. 1325707, 2024.
56. H.-R. Jiang and D.-C. Chan, "Superhydrophobicity on nanostructured porous hydrophilic material," Appl. Phys. Lett., vol. 108, no. 17, 2016.
57. M. A. Q. Siddiqui, S. Ali, H. Fei, and H. Roshan, "Current understanding of shale wettability: A review on contact angle measurements," Earth-Science Rev., vol. 181, pp. 1–11, 2018.
58. M. Tarek, W. Mahmoud, M. Elmosallamy, and ahmed El-Sherif, "Cadmium detection with nickel complex nanoparticles sensor using QCM technique Mohamed T. Radwan 1 , Walaa H. Mahmoud 1 , Mohamed A.F. ElMosallamy 2 and Ahmed A. El-Sherif 1," Bull. Fac. Sci. Zagazig Univ., vol. 2024, no. 1, pp. 132–142, 2024, doi: 10.21608/bfszu.2023.233505.1303.
59. L. Xuan, Z. Ju, M. Skonieczna, P. Zhou, and R. Huang, "Nanoparticles-induced potential toxicity on human health: applications, toxicity mechanisms, and evaluation models," MedComm, vol. 4, no. 4, p. e327, 2023.
60. J. Marrugo-Ramírez et al., "Nanomaterials-Based Wearable Biosensors for Healthcare," in Biosensors, CRC Press, 2022, pp. 345–379.
61. J. P. Mohamed and S. Gupta, "Artificial Intelligence-based Biosensors," in Cognitive Predictive Maintenance Tools for Brain Diseases, Chapman and Hall/CRC, pp. 112–125.
62. Z. Aksu, A. İ. Tatlı, and Ö. Tunç, "A comparative adsorption/biosorption study of Acid Blue 161: Effect of temperature on equilibrium and kinetic parameters," Chem. Eng. J., vol. 142, no. 1, pp. 23–39, 2008.
63. S. Mandal and S. Lahiri, "A review on extraction, preconcentration and speciation of metal ions by sustainable cloud point extraction," Microchem. J., vol. 175, p. 107150, 2022.
64. Y. C. López, G. A. Ortega, and E. Reguera, "Hazardous ions decontamination: From the element to the material," Chem. Eng. J. Adv., vol. 11, p. 100297, 2022.
65. A. M. Smith, The Ion Exchange and Sorption Properties of Microcrystals of Inorganic Oxides. University of Glasgow (United Kingdom), 1987.
66. R. Qiao and N. R. Aluru, "Ion concentrations and velocity profiles in nanochannel electroosmotic flows," J. Chem. Phys., vol. 118, no. 10, pp. 4692–4701, 2003.